Reduction of ecosystem productivity and respiration during the European summer 2003 climate anomaly: a joint flux tower, remote sensing and modelling analysis

Markus Reichstein, Philippe Ciais, Dario Papale, Riccardo Valentini, S. Running, Nicolas Viovy, Wolfgang Cramer, A. Granier, J. Ogée, Vincent Allard, et al.

Reduction of ecosystem productivity and respiration during the European summer 2003 climate anomaly: a joint flux tower, remote sensing and modelling analysis

M. Reichstein[2,3], P. Ciais[4], D. Papale[1], R. Valentini[1], S. Running[5], N. Viovy[4], W. Cramer[3], A. Granier[6], J. Ogée[7], V. Allard[8], M. Aubinet[9], C. Bernhofer[10], N. Buchmann[11], A. Carrara[12], T. Grünwald[10], M. Heimann[2], B. Heinesch[9], A. Knohl[2,13], W. Kutsch[2], D. Loustau[7], G. Manca[1], G. Matteucci[14], F. Miglietta[15], J.M. Ourcival[16], K. Pilegaard[17], J. Pumpanen[18], S. Rambal[16], S. Schaphoff[2], G. Seufert[19], J.-F. Soussana[8], M.-J. Sanz[12] , T. Vesala[20], M. Zhao[5]

[1]Department of Forest Environment and Resources, DISAFRI, University of Tuscia, Viterbo, Italy
[2]Max Planck Institute for Biogeochemistry, Postfach 10 01 64, 07701 Jena, Germany
[3]Potsdam Institute for Climate Impact Research, Telegrafenberg C4, D-14473 Potsdam, Germany
[4]Laboratoire des Sciences du Climat et de l'Environnement, LSCE, 91191, Gif sur Yvette, France
[5]NTSG, Department of Ecosystem and Conservation Sciences, University of Montana, USA
[6]Ecologie et Ecophysiologie Forestières, Centre de Nancy, 54280 Champenoux, France
[7]Functional Ecology and Environmental Physics, Ephyse, INRA, Villenave d'Ornon, France
[8]Grassland Ecosystem Research, INRA, Site de Crouel. 234, Clermont-Ferrand, F-63039, France
[9]Faculté des Sciences Agronomiques, Av. de la Faculté d'Agronomie 8, B-5030 Gembloux Belgique
[10]Department of Meteorology, Institute of Hydrology and-Meteorology, Technische Universität Dresden, D-01062 Dresden
[11]Institute of Plant Sciences, Universitätsstrasse 2, ETH Zentrum LFW C56, CH-8092 Zuerich, Switzerland
[12]Fundacion CEAM C/ Charles Darwin, Parque Tecnologico de Paterna, 46980 Valencia, Spain
[13]Department. of ESPM, Ecosystem Science Division, University of California, Berkeley, CA, USA
[14]CNR-ISAFOM, Via Cavour, 4-6 I-87036 Rende (CS), Italy
[15]IBIMET-CNR, Ple delle Cascine, 18, 50144 Firenze, Italy
[16]Dream CEFE-CNRS, 1919 route de Mende, 34293 Montpellier, France
[17]Plant Research Department, Risø National Laboratory, 4000 Roskilde, Denmark
[18]Department of Forest Ecology, University of Helsinki, PO Box 24, Helsinki, FN 0014, Finland
[19]Institute for Environment and Sustainability, Joint Research Center European Commission, TP 280, I-21020 Ispra, Italy
[20]Department of Physical Sciences, University of Helsinki, PO Box 64, Helsinki, Finland

The European CARBOEUROPE/FLUXNET monitoring sites, spatial remote sensing observations via the EOS-MODIS sensor and ecosystem modelling provide independent and complementary views on the effect of the 2003 heatwave on the European biosphere's productivity and carbon balance. In our analysis, these data streams consistently demonstrate a strong negative anomaly of the primary productivity during the summer of 2003. FLUXNET eddy-covariance data indicate that the drop in productivity was not primarily caused by high temperatures ('heat stress') but rather by limitation of water (drought stress) and that, contrary to the classical expectation about a heat wave, not only gross primary productivity but also ecosystem respiration declined by up to more than to 80 gC m^{-2} $month^{-1}$. Anomalies of carbon and water fluxes were strongly correlated. While there are large between-site differences in water-use efficiency (WUE, 1–6 kg C kg^{-1} H_2O) here defined as gross carbon uptake divided by evapotranspiration (WUE=GPP/ET), the year-to-year changes in WUE were small (<1 g kg^{-1}) and quite similar for most sites (i.e. WUE decreased during the year of the heatwave). Remote sensing data from MODIS and AVHRR both indicate a strong negative anomaly of the fraction of absorbed photosynthetically active radiation in summer 2003, at more than five standard deviations of the previous years. The spatial differentiation of this anomaly follows climatic and land-use patterns: Largest anomalies occur in the centre of the meteorological anomaly (central Western Europe) and in areas dominated by crops or grassland. A preliminary model intercomparison along a gradient from data-oriented models to process-oriented models indicates that all approaches are similarly describing the spatial pattern of ecosystem sensitivity to the climatic 2003 event with major exceptions in the Alps and parts of Eastern Europe, but differed with respect to their interannual variability.

Correspondence: Markus Reichstein, Biogeochemical-Model-Data Integration Group, Max-Planck Institute for Biogeochemistry, 07701 Jena, Germany, fax: + 49 3641 576200, e-mail: mreichstein@bgc-jena.mpg.de

Keywords: carbon balance, eddy covariance, drought, climate change, ecosystem productivity, ecosystem modelling

Introduction

Monitoring of the earth system and its biosphere in the context of global change should involve a well-balanced and interlinked combination of observation systems (remote sensing, ground-based networks) and data- and process-oriented modelling. Observation systems of the terrestrial biosphere have received a strong development during the last decades. The global FLUXNET network of eddy covariance towers provides continuous half-hourly estimates of ecosystem CO_2 and H_2O exchange for 10 years and encompasses more than 200 sites (Baldocchi *et al*., 2001). The moderate resolution imaging spectrometer (MODIS) sensor has been providing high-precision and quality-controlled daily spectral reflectance information about the land surface at 250–1000 m resolution for 5 years (Myneni *et al*., 2002), extending the 20 year-long time-series of the NOAA-AVHRR sensor, that was originally designed for the observation of the atmosphere and not the biosphere (Tucker *et al*., 1985). In parallel to this development of observational systems, a coevolution of modelling approaches ranging from statistical techniques to ecosystem process models of different complexity has taken place (e.g., Hunt *et al*., 1996; Thornton *et al*., 2002; Papale & Valentini, 2003; Reichstein *et al*., 2003c; Sitch *et al*., 2003; Dijk *et al*. 2005; Krinner *et al*., 2005). Process models are mostly developed to represent nonlinear mechanisms of the (coupled) carbon, water and nutrient cycles in a prognostic mode while data-oriented approaches are profitably used for diagnostic and exploratory purposes.

The European 2003 summer heatwave had significant impacts on European ecosystems, including large losses in agriculture. However, from a scientific perspective the European 2003 summer heatwave provided the opportunity to test the different observing and modelling systems' ability to characterize the biosphere's response to climate anomalies. A combined, integrated analysis should reveal where consistent, complementary or contradictory results are obtained via remote sensing, ground observation and modelling approaches. While a number of the biosphere's processes and properties potentially respond to climate anomalies we here concentrate on CO_2 and H_2O fluxes and on the biosphere's absorption of photosynthetically active radiation. In extension of parallel studies (Ciais *et al*., 2005; Granier *et al*., 2005), we specifically address the following questions: How exceptional was the decrease of the vegetation's ability to absorb radiation as observed from space? Which climatic factor dominated the ecosystems' response to the summer 2003 climate anomaly? How strong was the link between carbon and water cycles in their reaction to the climate anomaly? To what degree did the different modelling approaches agree in their predictions of the response of ecosystem fluxes to the 2003 anomaly?

Material and methods

Remote sensing data

In this analysis we have used the eight daily composite estimates of the fraction of absorbed photosynthetically active radiation (fAPAR) from the MODIS sensor onboard the EOS-Terra platform for the years 2000–2004 at 1 km resolution (MOD15A2, collection 4 data; cf. Myneni *et al*., 2002). These fAPAR data were filtered according to the associated quality flag that indicates problems with the retrieval of the fAPAR data due to atmospheric conditions (clouds, aerosols), instrument problems or saturation. Two levels of quality filtering were chosen; first only best retrievals by the main algorithm (QC-flag = 0) were accepted, secondly also cloud free retrievals by the empirical back-up algorithm (also QC-flag = 33 and 97 accepted). Data gaps appearing through this filtering were filled using linear temporal interpolation. Subsequently, the fAPAR time series were subject to a treatment with the best index slope extraction (BISE) algorithm with a window size of two time steps (Viovy & Arino, 1992) to remove occasional ($<10\%$ of the data) sudden spikes of MODIS fAPAR data likely caused by atmospheric effects not indicated by the quality control flag. A typical example of the data treatment is shown for two eddy covariance sites with stable fAPAR in Fig. 1. Finally, the fAPAR values were spatially aggregated into blocks of 10×10 pixels, while accounting for different vegetation types.

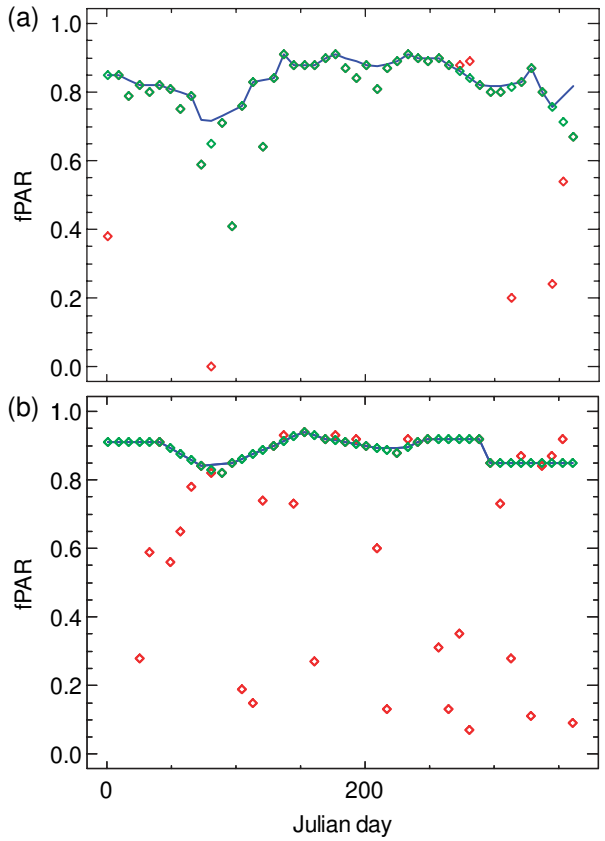

Fig. 1 Example of processing the moderate resolution imaging spectrometer (MODIS) fraction of absorbed photosynthetically active radiation (fAPAR) product for two evergreen sites (a, Puéchabon, evergreen broadleaf oak forest, France; b, Tharandt, evergreen needle-leaf spruce forest Germany). Red dots show original MODIS fAPAR data flagged as cloud-contaminated, green dots are MODIS fAPAR flagged as without clouds effects, and the blue line is the interpolated/smoothed time-series.

This resulted in average fAPAR values for each vegetation type in each aggregated $10 \times 10\,\mathrm{km}^2$ pixel. The IGBP vegetation classification at 1 km resolution according to the MODIS classification (MOD12Q1) was used (Friedl *et al.*, 2002).

In addition to the 5-year long MODIS fAPAR data set, the AVHRR-GIMMS fAPAR data set at 0.25° spatial and monthly temporal resolution was analysed (Zhou *et al.*, 2003). At the time of the analysis only data from 1982 to 2002 was available. As fAPAR estimates from MODIS and from AVHRR are not directly comparable (different spectral response of the sensors and different processing) and a generalized harmonization of the MODIS and AVHRR time series is still undertaken, a statistical intercalibration of MODIS and AVHRR time series was performed using the overlapping years 2000–2002. For each month in that period the regression coefficients (a_0–a_3) of the polynomial equation

$$\begin{aligned}\mathrm{fAPAR}_{\mathrm{MODIS}}(i,j) = & a_0 + a_1 \mathrm{fAPAR}_{\mathrm{GIMMS}}(i,j) \\ & + a_2 \mathrm{fAPAR}^2_{\mathrm{GIMMS}}(i,j) \\ & + a_3 \mathrm{fAPAR}^3_{\mathrm{GIMMS}}(i,j),\end{aligned} \quad (1)$$

were estimated with a least squares regression algorithm (Visual_Numerics_Inc. 2001) by regressing all European pixels (column i, row j), where both MODIS and AVHRR-GIMMS fAPAR retrievals were available. The coefficients of determination for the regression were between 0.50 and 0.65 for the winter half year (October–March) and 0.70 and 0.85 for the summer half year (April–September). The regression coefficients differed between months, but were similar in all 3 years, and indicate on average by 0.1 units lower fAPAR values in the AVHRR data set, in the range of fAPAR 0.2–0.7 during the summer months and smaller biases under different conditions. Hence, the whole AVHRR-GIMMS fAPAR time series was subsequently adjusted towards the MODIS fAPAR using monthly varying coefficients, i.e.

$$\begin{aligned}&\mathrm{fAPAR}^{\mathrm{adjusted}}_{\mathrm{GIMMS}}(i,j,m,y) \\ &\quad = a_0(m) + a_1(m)\mathrm{fAPAR}_{\mathrm{GIMMS}}(i,j,m,y) \\ &\qquad + a_2(m)\mathrm{fAPAR}^2_{\mathrm{GIMMS}}(i,j,m,y) \\ &\qquad + a_3(m)\mathrm{fAPAR}^3_{\mathrm{GIMMS}}(i,j,m,y),\end{aligned} \quad (2)$$

where indices i and j denote the spatial position of the pixel, m the month and y the year. With respect to the central tendency, the adjusted $\mathrm{fAPAR}_{\mathrm{GIMMS}}$ time-series is considered as being statistically harmonized with the MODIS time series for the European domain.

CO_2 and H_2O flux and meteorological data

The ecosystem–atmosphere CO_2 and H_2O exchange data have been collected at different sites mostly from within the CARBOEUROPE ecosystem flux component (Table 1). We chose the years 2002–2003 and analysed differences in summer fluxes between these 2 years. The choice of 2002 as a reference year of course is somewhat arbitrary and does not allow using the term anomaly in a strict sense. However, the years 2002–2003 provided a homogeneous data set with a maximal spatial coverage. Moreover, except for precipitation in Eastern Germany and Northern Italy the year 2002 was very similar to the average conditions over the previous 30 years and thus can serve as a proxy for 'normal' climatic conditions.

Half-hourly meteorological conditions (global, net and PPFD radiation, air temperature and humidity, rainfall, wind speed and direction) were measured above all stands. Half-hourly fluxes of CO_2 and H_2O were calculated from the high-frequency data according to Aubinet *et al.* (2000), including storage correction and

Table 1 Summary of the eddy covariance sites analysed in this study

Site code	Name	Vegetation (IGBP)*, main genus	Country	Lat (°)	Lon (°)	Max LAI ($m^2\,m^{-2}$)	Stand age (years)	Annual mean T_{air} (°C)	Mean annual P (mm)	ΔT_{air} (°C)	ΔP (mm $month^{-1}$)	ΔGPP (g C m^{-2} $month^{-1}$)	ΔTER (g C m^{-2} $month^{-1}$)	ΔNEP (g C m^{-2} $month^{-1}$)	ΔET (mm-$month^{-1}$)
El	El Saler	ENF, pine	SP	39.28	0.33	3.1	>100	17.1	449	1.7	−55	−33	−63	30	n.d.
Ca	Castelporziano	EBF, oak	IT	41.71	12.38	3.5	56	15.6	781	3.5	−43	−47	−21	−26	−13
Ro	Roccarespampani	DBF, oak	IT	42.39	11.92	3.8	20	14.4	936	2.3	−87	−117	−89	−28	−21
Sa	San Rossore	ENF, pine	IT	43.71	17.28	4.2	44	14.2	920	1.8	−77	−87	−47	−40	−16
Br	Bray	ENF, pine	FR	44.72	−0.77	4.8	38	12.9	955	2.9	−2	29	21	8	26
La	Laqueuille	GRA, poa	FR	45.64	2.75	3.0	n.a.	8.0	1300	3.5	−15	−25	−19	−6	n.d.
Pi	Pianosa	OSH, junip.	IT	42.58	10.07	3.5	n.a.	16.1	477	3.2	−30	5	9	−4	−19
Pu	Puéchabon	EBF, oak	FR	43.73	3.58	2.9	58	13.4	883	2.2	−42	−52	−24	−28	n.d.
He	Hesse	DBF, beech	FR	48.67	7.08	6.7	37	9.2	885	2.0	−34	−115	−42	−73	−17
Vi	Vielsalm	MF, fir	BE	50.30	6.00	5.1	90	7.5	1000	1.4	−25	−20	−37	+17	11
Th	Tharandt	ENF, spruce	GE	50.95	13.57	7.0	110	7.5	820	1.0	−58	−41	−10	−31	−8
Ha	Hainich	DBF, beech	GE	51.07	10.5	5.0	250	7.0	750	1.8	−43	−82	−25	−57	−8
So	Soroe	DBF, beech	DK	55.48	11.63	4.8	80	8.1	510	0.3	−47	−15	−14	−1	5
Hy	Hyytiälä	ENF, pine	FI	61.85	24.28	3.0	42	3.5	640	−0.1	−15	−3	10	−13	−3

*Vegetation type according to IGBP classification (ENF: Evergreen needle-leaf forest; EBF: Evergreen broad-leaf forest; DBF: deciduous broad-leaf forest; GRA: grassland; MF: mixed forest; OSH: open shrubland).

Lat, latitude; Lon, longitude; max LAI, maximum leaf area index; T_{air}, air temperature; P, precipitation; GPP, gross primary productivity; TER, terrestrial ecosystem observation; NEP, net ecosystem productivity; ET, evapotranspiration. Δ, difference of the respective quantity in July–September between 2003 and 2002, except for precipitation that is for June–August to account better for lag effects; n.a., not applicable (no forest); n.d., not determined or more than 20% gaps in 2002 or 2003.

filtering of low-turbulence conditions during night using a u^*-threshold criterion. u^*-thresholds varied site-specifically between 0.1 and 0.4 $m\,s^{-1}$. The same procedure of gap filling was applied at all sites and the same method for calculating ecosystem respiration (TER) and gross photosynthesis (GPP) from net CO_2 fluxes (NEE) was used (Reichstein *et al*., 2005). The partitioning of the observed NEE into GPP and TER was achieved through an algorithm that first establishes a short-term temperature dependence ecosystem respiration from turbulent night-time data and then uses this relationship for extrapolating respiration from nighttime to daytime. Day-to-day varying base rates of respiration were derived from the u^*-filtered night-time fluxes. The algorithm avoids the confounding effect of covariance between general biological activity and temperature. Uncertainties of the changes of GPP and TER between the years were estimated as a combination of the uncertainties that arise from the eddy covariance measurements themselves, the u^*-filtering, the gap-filling and the flux-partioning according to the following reasoning. We assume that potential systematic errors that affect the absolute magnitude of the fluxes (e.g. occurrence of advection), as well as uncertainties by the u^*-filtering do not affect estimates of between-year variability, as fluxes in different years should be affected similarly. Random errors of up to 50% for the half-hourly flux, decline by integration over a month or a year (Goulden *et al*., 1996). The bias of the gap-filling was estimated by introducing artificial gaps and was never higher than $0.1\,\mu mol\,m^{-2}\,s^{-1}$. As at maximum 20% of the data were gap-filled if flux integrals were reported, this corresponds to an error of $0.6\,g\,C\,m^{-2}\,month^{-1}$. The uncertainty of the flux-partitioning is largely determined by the uncertainty of the temperature sensitivity (E_0 parameter in Lloyd & Taylor, (1994)) used to extrapolate from night to day. This uncertainty was estimated as the standard deviation of all E_0 estimates for 1 year (cf. Reichstein *et al*., 2005), assuming that the expected value of E_0 is constant over the year and all variability can be attributed to the estimation error. Clearly, as E_0 can vary through the year, this is a conservative estimate of error. Errors for each year were summed for the difference between years, assuming that they are independent between years. These uncertainties remained between 4 and $17\,g\,C\,m^{-2}\,month^{-1}$ for the summer months and between 25 and $95\,g\,C\,m^{-2}$ for the whole year.

Water-use efficiencies (WUE) as an important integrative variable of canopy and ecosystem function have also been calculated on half-hourly, daily and monthly basis. WUE of gross carbon uptake were calculated by dividing time integrals of GPP by the respective H_2O flux integrals (e.g. over daily, monthly or seasonal intervals). Please note that such definition of ecosystem level WUE also includes evaporation of canopy interception and soil evaporation that might confound direct conclusions on canopy function. Similar to carbon fluxes, water flux estimates from eddy covariance may be subject to systematic errors, as often revealed by insufficient closure of the energy balance. Hence, systematic errors of up to 20% regarding absolute WUE cannot be excluded (Wilson *et al*., 2002), but again changes between years that we focus on, should be less affected if the bias is similar in 2 years and partly cancels out by differencing.

Modelling approaches

Four different and largely independent modelling systems were used to estimate the effect of the heatwave on the European terrestrial biosphere's carbon balance components as summarized in Table 2. As we wanted to explore the full range of independent modelling systems (including model and driving data) we put up with the fact that at this stage a formal intercomparison of the models themselves (without the driving data) is not possible. Differences between modelling systems can be caused by the models themselves or by the input data and can, thus, be considered as conservative estimates. The models being used can be arranged along a continuum from process-oriented to data-oriented approaches and are shortly described

1. The ORCHIDEE model (Krinner *et al*., 2005) can be considered as the most process-oriented model, treating processes explicitly from half-hourly to decadal time scales. It is a dynamic global vegetation model (DGVM) designed to be coupled with ocean–atmosphere circulation models in order to simulate the global carbon and water cycles. It distinguishes 12 plant functional types (PFTs), mostly taken from the LPJ model but with two additional types for agro-systems (C3 and C4 types) and describes all the major processes related to the carbon and water cycles in terrestrial ecosystems (air-to-leaf CO_2 diffusion, photosynthesis, respiration, allocation, growth, phenology, mortality, mineralization; rain interception, evapotranspiration, drainage, water routing), combined with a single-energy budget equation. Plant structure is represented by five functionally different parts (foliage, stems, branches, coarse and fine roots) and a carbohydrate storage compartment is also considered for broadleaf species. The allocation in ORCHIDEE dynamically calculates the fraction of assimilates to be allocated to the different plant parts taking into account environmental influences (light availability, temperature and soil water) according to the allocation scheme of Friedlingstein *et al*. (1999). Phenology is fully prognostic, based on

Table 2 Overview of modelling approaches employed in this study

	Driving variables used					
Name	Variables (source)	Spatial resolution	Temporal resolution	Vegetation classes	Soil	Remarks
ORCHIDEE	Global radiation, air temperature, wind speed, vapour pressure deficit, precipitation (ECMWF)	$0.3^\circ \times 0.3^\circ$ latitude–longitude grid	Half-hourly	Eight forest classes, C3/C4 natural graminoids, C3/C4 agricultural graminoids	FAO soil map texture information	Spin-up run, then transient from 1954
LPJ_{nat}	Global radiation, air temperature, precipitation, number of wet days (CRU)	$0.5^\circ \times 0.5^\circ$ latitude–longitude grid	Monthly, downscaled to daily	Eight forest classes, 2 graminoids	FAO soil map texture information	Spin-up run, then transient from 1901
MOD17	Global radiation, minimum air temperature, average air temperature, mean daytime vapour pressure deficit (DAO), fAPAR (MODIS, cf. text)	$10 \times 10\,km^2$ sinusoidal (downscaled from $1^\circ \times 1^\circ$ for meteorology; aggregated from $1 \times 1\,km^2$ for fAPAR)	Daily	IGBP vegetation classes according to MODIS (cf. text)	ignored	Model parameterized with eddy covariance data 2001–2002
ANN						Network trained with eddy covariance data 2001–2002

fAPAR, fraction of absorbed photosynthetically active radiation; MODIS, moderate resolution imaging spectrometer.

growing degree days, chilling or soil water content indexes specific to each PFT and calibrated with remote-sensing data (Botta *et al*., 2000).

2. The LPJ-DGVM (Sitch *et al*., 2003) simulates processes at daily to decadal time scales. It is one of a family of models derived from the BIOME terrestrial biosphere model (Prentice *et al*., 1992). The model simulates the distribution of 10 PFTs with different physiological (C3 or C4 photosynthesis), phenological (deciduous, evergreen) and physiognomic (tree, grass) attributes, based on bioclimatic limits for plant growth and regeneration and plant specific parameters that govern plant competition for light and water.

Photosynthesis is calculated as a function of absorbed photosynthetically active radiation, temperature, atmospheric CO_2 concentration, day length and canopy conductance using a form of the Farquhar scheme (Farquhar & Von Caemmerer, 1982; Collatz *et al*., 1991) with canopy-level optimized nitrogen allocation (Haxeltine & Prentice, 1996) and an empirical convective boundary layer to couple the C and H_2O cycles (Monteith, 1995). Soil hydrology is simulated using two soil layers (Haxeltine *et al*., 1996).

Annual NPP is allocated to the four carbon pools (representing leaves, sapwood, heartwood and fine-roots) of each PFT population on the basis of allometric relationships linking height, diameter and the leaf-area to sapwood area ratio to these pools. Litterfall from vegetation enters separate above- and belowground litter pools, which themselves provide input to a fast and a slow decomposing soil carbon pool. Decomposition rates of soil and belowground litter organic carbon depend on soil temperature and soil moisture (Lloyd & Taylor, 1994; Foley *et al*., 1996). Vegetation dynamics are modelled based on light competition, fire disturbance, reestablishment rates, and a set of temperature-related limits to survival or establishment (Sitch *et al*., 2003).

3. As a semiempirical relatively data-oriented model a successor of a remote sensing driven radiation-use efficiency model was used (Nemani *et al*., 2003).

$$\mathrm{GPP} = \varepsilon \times \mathrm{fAPAR} \times \mathrm{PAR}, \tag{3}$$

where PAR is the photosynthetically active radiation flux ($MJ\,m^{-2}\,day^{-1}$), fAPAR is the fraction absorbed by the vegetation, and ε is the conversion efficiency of energy to fixed carbon ($g\,C\,MJ^{-1}$) according to Eqn (3),

$$\varepsilon = \varepsilon_{\max} f_1(T_{\min}) f_2(\mathrm{VPD}), \tag{4}$$

where $\varepsilon_{\max}$ is the vegetation-specific maximum conversion efficiency. The functions f_1 and f_2 (between 0 and 1) describe the influence of meteorological conditions on ε with $T_{\min}$ being the daily minimum air temperature and VPD the daytime average vapour pressure deficit. While these functions were left as in the original

parameterization the maximum radiation-use efficiency (ε_{max}) was optimized vegetation specifically against available European eddy covariance data from the CARBOEUROPE network (Reichstein *et al*., 2004).

Ecosystem respiration was estimated with a semiempirical model modified from (Reichstein *et al*., 2003b):

$$R_{eco} = [R_0 + (1 - e^{-k_1 \mathrm{LAI}_{max}})R_1 + (1 - e^{k_2 \mathrm{GPP}})R_2] \times e^{E_0\left(\frac{1}{T_{ref}-T_0}-\frac{1}{T-T_0}\right)} \frac{P+P_0}{k+P+P_0}, \quad (5)$$

where LAI_{max} is the maximum leaf area index at the site ($m^2\,m^{-2}$), GPP is the gross primary productivity from Eqn (3) ($g\,C\,m^{-2}\,day^{-1}$), T (°C) is the average air temperature and P is the precipitation of the last 30 days (mm). The other quantities are model parameters describing the assumed functional dependency of the quantities. Compared with the previously published model on soil respiration (Reichstein *et al*., 2003b), a short-term dependency of R_{eco} on GPP is added and the temperature dependency is changed from Q_{10} model to the Arhennius type of equation. The parameters were derived using eddy covariance ecosystem respiration data that have been derived according to the methods in Reichstein *et al*., 2005. As in the original model, in this analysis the parameters are assumed to be independent of vegetation cover (and forest sites are overrepresented in the used eddy covariance data sets).

4. A completely data-oriented modelling approach was pursued by the application of artificial neural networks (ANN) according to Papale and Valentini (2003). ANNs are composed of simple elements, organized in layers and operating in parallel. These elements are inspired by biological nervous systems. As in nature, the network properties are determined largely by the connections between elements. We can train a neural network to perform a particular function by adjusting the values of the connections (weights) between elements. Commonly neural networks are adjusted, or trained, so that a particular input leads to a specific target output. There, the network is adjusted, based on a comparison of the output and the target, until the network output matches the target. Typically many such input/target pairs are used, in this supervised learning, to train a network.

ANNs are strongly dependent by the data used for the training that should be representative of the domain. In this application GPP, NEE and TER measured at the eddy covariance sites during the years 2001–2002 were used as output to assess in the ANN training. There were sufficient data only from two grassland sites and one cropland site available; hence it was impossible to apply the ANNs to these two land cover classes. Different feed-forward backpropagation neural networks were trained for deciduous and evergreen forests, in both cases using a Levenberg–Marquardt training algorithm. The ANNs' architectures were chosen on the basis of the performances obtained using networks with different structures (one hidden layer with a number of nodes from four to eight nodes and two hidden layers with four and three nodes) and for all the networks an architecture with one hidden layer and eight nodes were selected, with sigmoidal transfer functions for all the connections. The inputs (predictor variables) included global radiation, air temperature, vapour pressure deficit, MODIS-derived fAPAR values at the respective site pixels, that were obtained as described above, and two season indicator variables that are calculated as the sine and cosine of the day of the year (DOY)

$$\mathrm{seas1} = \frac{1}{2}\left[\cos\left(\frac{2\pi \mathrm{DOY}}{365}\right) + 1\right],$$
$$\mathrm{seas2} = \frac{1}{2}\left[\sin\left(\frac{2\pi \mathrm{DOY}}{365}\right) + 1\right]$$

and help the network to 'understand' the seasonality (Scardi, 2001).

Inputs and outputs were rescaled between −1 and + 1 and the early stopping technique was used to avoid overfitting and improve generalization (Demuth & Beale, 2001) The initial connections weights were chosen randomly and 20 networks were trained using different sets of weights. The data sets used in the ANNs training were divided in three subset, training, test and validation sets, with the last one that is not used at all in the training phase but only to assess the ANN generalization ability. In Table 3, the summary of the different ANNs' performances on the validation set is shown.

Table 3 Summary of the ANNs performances on the validation set: *m*, *b* and *r* are respectively slope, intercept and regression values of the linear regression between each element of the network response and the corresponding target

Land cover	Variable	*M*	*b*	*r*	RMSE	MAE
Evergreen	GPP	1.01	0.032	0.91	1.215	0.88
	NEE	1.036	0.045	0.848	1.043	0.775
	TER	1.001	0.000	0.879	0.746	0.542
Deciduous	GPP	0.987	0.044	0.979	0.982	0.656
	NEE	0.987	0.016	0.956	1.033	0.718
	TER	0.979	0.05	0.957	0.538	0.398

RMSE, root mean square error ($g\,C\,m^2\,day^{-1}$); MAE, mean absolute error ($g\,C\,m^2\,day^{-1}$).
Number of example used to built the Training (*Tr*), Test (*Ts*) and Validation (*Vl*) sets: Evergreen *Tr* = 2282, *Ts* = 1140, *Vl* = 1141; Deciduous *Tr* = 981, *Ts* = 490, *Vl* = 490.

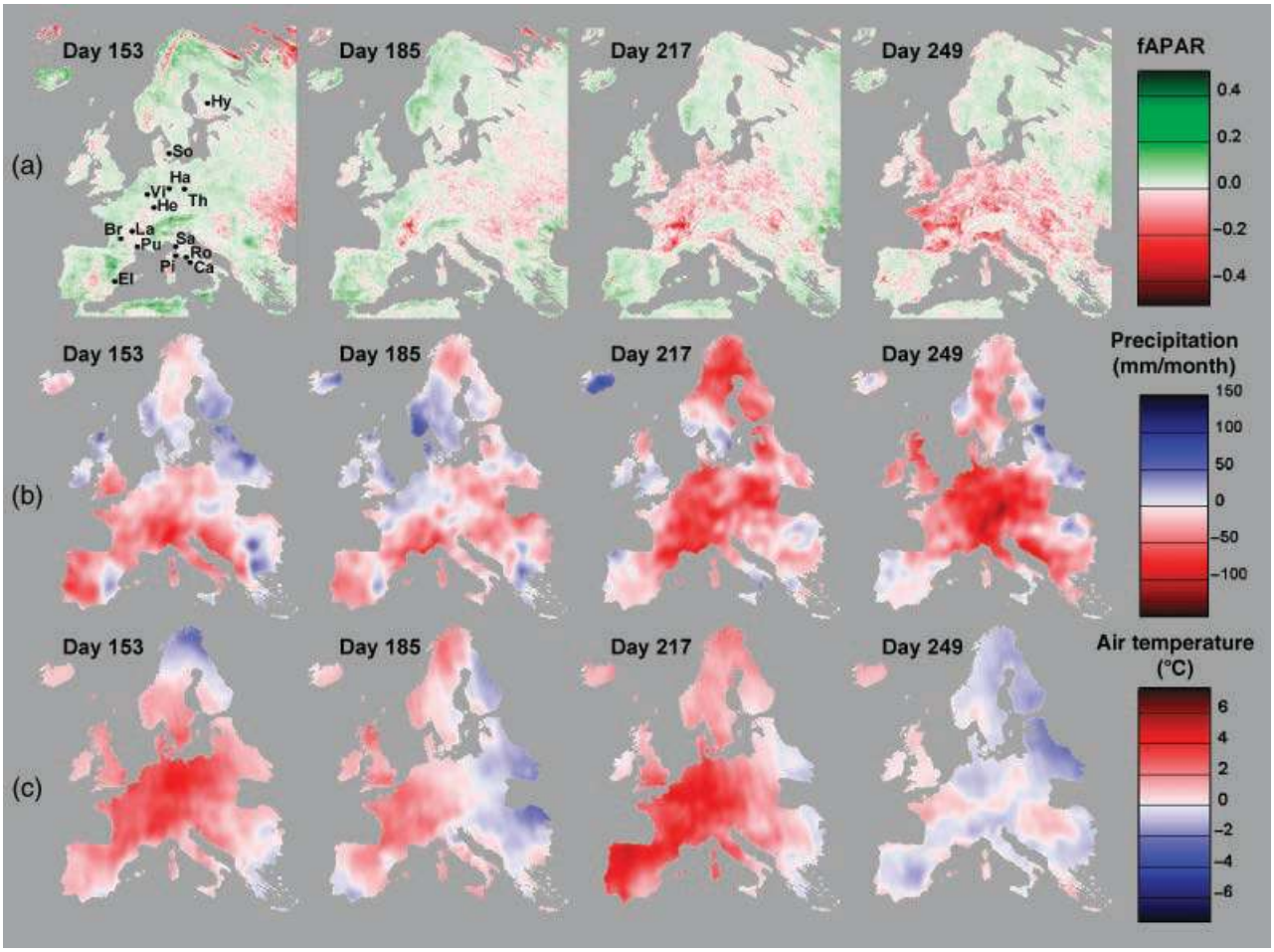

Fig. 2 Temporal development (from left to right) of the anomaly spatial pattern of (a) the fraction of absorbed photosynthetically active radiation (fAPAR), (b) precipitation and (c) air temperature during 2003 from June (day 153) to September (day 249). Anomalies are expressed as absolute differences in between 2003 and the mean of the years 2002, 2001, 2002 and 2004. Anomalies for fAPAR concern the instantaneous fAPAR values at that day, for precipitation the cumulative precipitation over the 60 days before, and for air temperature the average over a 20-day window around the day. See legend to the right for colour coding of anomalies, maps are in sinusoidal projection with central meridian at 0°.

For each output (GPP, NEE and TER) and land cover (deciduous and evergreen) the ANN with the best performance was selected and applied at continental scale using the same input used for the MOD17 model. In the 19 land-use classes used in the MODIS classification (MOD12Q1) there is also a 'mixed forest' class that was impossible to use as separated class for the same reason of grassland and cropland (not enough data to train a specific network). For this analysis, we considered the mixed forest as composed by 50% evergreen and 50% deciduous.

Results and Discussion

The remote sensing observation with the MODIS sensor allows drawing a spatially and temporally highly resolved picture of the European's biosphere reaction to the heat and drought in summer 2003 using the fAPAR as one indicator of the biosphere's state (Fig. 2). The earliest and strongest occurrence of an fAPAR reduction occurs in central southern France and reaches its maximum in central Western Europe at the beginning of September ('julday 249'). This late occurrence of the maximum reduction (and not during July/August when highest temperature anomalies occurred) indicates that the biosphere reacted delayed or to some cumulative and not instantaneous quantity. Remarkable are the quite distinct geographical boundaries that separate regions with a reduction of fAPAR from regions that exhibit no change or an increase of fAPAR (Iberian Peninsula, Central Alps, Skandinavia). Areas exhibiting no fAPAR reduction are either regions where

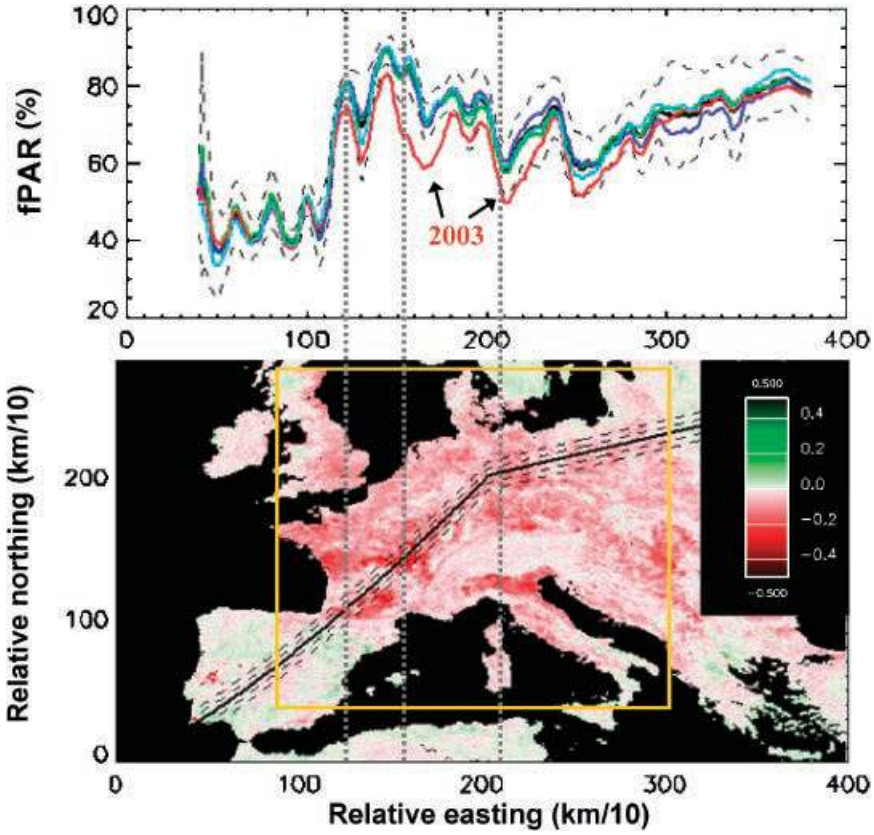

Fig. 3 (a) Estimated mean July–September fraction of absorbed photosynthetically active radiation (fAPAR) from moderate resolution imaging spectrometer along the transect indicated in (b) during the years 2000–2004 (color lines). The dashed black lines ± 5 standard deviations around the mean over all years except 2003. Dotted vertical lines indicate position local minima of the anomaly in 2003. (b) shows the spatial pattern of the average July–September fAPAR anomaly and contains the position of the transect band (solid and outer dotted lines). The rectangle denotes the domain used for averaging in Fig. 4. Anomalies are expressed as in Fig. 2.

the climate anomaly was also minor (Spain, Portugal, Scandinavia, cf. Schär *et al*., 2004), or favourable for the biosphere (Alps, cf. Jolly *et al*., 2005). An exception to this general pattern is however seen in central Portugal where strong local negative anomalies occur. These anomalies are however not a direct climate effect, but are deviations from the normal vegetation cover through major forest fires that occurred in 2003 in Portugal. Along large parts of the transect in Fig. 3 particularly from the Pyrenees to the German–Polish border the average July–September 2003 fAPAR deviated by more than five standard deviations from the mean observed during the same time in 2000–2002 and 2004. In the Iberian Peninsula and towards the Ural 2003 summer fAPAR seems well within the year-to-year variability. Since 5 years of MODIS remote sensing data maybe considered not sufficient for the calculation of an anomaly, we extended the MODIS time series with NOAA-AVHRR-GIMMS fAPAR retrievals (Fig. 4). Even at a continental scale, the 2003 fAPAR is uniquely low compared with the 20 years before and outside five standard deviations both of the MODIS and the GIMMS mean. Assuming Gaussian-distributed values this corresponds to an average return interval of more than 10^6 years, or to more than 142 years in case of log-normally distributed fAPAR, which stresses the extreme fAPAR signal detected via remote sensing. The recovery of the fAPAR during 2004 indicates that on average no continental scale carry-over effect of the 2003 drought to 2004 on phenology are detected via MODIS remote sensing. Yet, local effects cannot be excluded and have already been detected in southern France, where 38 500 ha of *Quercus ilex* forest surrounding the Puéchabon flux site have been totally or partly defoliated by gypsy moth caterpillars *Lymantria dispar* L. (Joffre *et al*., 2005), although a direct link to the 2003 heat and drought is hard to establish.

The fAPAR of different vegetation types were differently affected by the 2003 climate anomaly in the different countries (Fig. 5a). Herbaceous vegetation (crops and grassland) show the strongest relative change in fAPAR in all countries, positive in Portugal

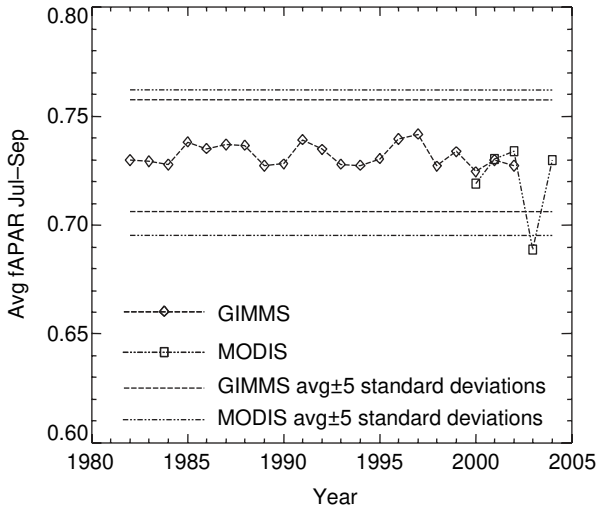

Fig. 4 Average July-to-September fraction of absorbed photosynthetically active radiation (fAPAR) for the continental rectangular domain indicated in Fig. 3 for each year from AVHRR-GIMMS (1982–2002) and moderate resolution imaging spectrometer (2000–2004). The average ±5 standard deviations of each time-series excluding year 2003 are indicated by the horizontal lines.

(P) and Spain (E), and negative in the other countries. This is expected as grasses tend to exhibit alterations of photosynthetic pigments and thus a respective change in spectral characteristics ('yellowing'). The countries Germany (D) and France (F) that were most strongly affected by the heatwave, also show the strongest reduction in fAPAR for crops and grassland. Here, forest fAPAR was clearly less affected in the order deciduous > mixed > evergreen forest, as might also be expected from the spectral stability of the respective leaves (Wang *et al*., 2004). It should be noted that the reduction of fAPAR, in the forest pixel cannot be simply attributed to a change of absorption of the tree leaves, but can also occur via effects on the understorey, heterogeneous or even misclassified pixels (containing fractions of grass vegetation). This seems to be a problem in the Netherlands (NL) where evergreen forests exhibit higher reductions than the deciduous, that might be caused by yellowing of *Deschampsia flexuosa* grass, that is particularly abundant in Dutch Pine forest on acid soils (Persson *et al*., 2000). As mentioned earlier, the effect of the 2003 fires on forest fAPAR is detected in Portugal. The modeled relative change in fAPAR by the

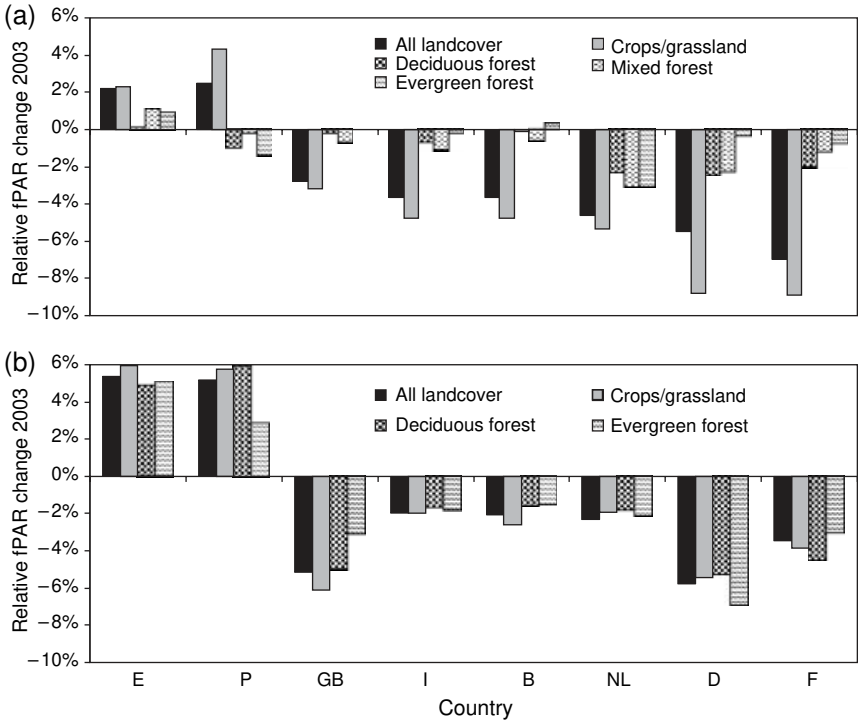

Fig. 5 Relative difference of 2003 vs. 2000, 2001, 2002 and 2004 July-to-September fraction of absorbed photosynthetically active radiation (fAPAR) for selected countries and vegetation classes. The relative difference is defined as $[fAPAR_{2003} - avg(fAPAR_{2000,\ 2001,\ 2002,\ 2004})]/avg(fAPAR_{2000,\ 2001,\ 2002,\ 2004})]$ where avg denotes the arithmetic mean operation. (a) is observed for moderate resolution imaging spectrometer (MODIS) fAPAR by MODIS-IGBP vegetation classes; (b) is model output from the ORCHIDEE model for plant functional types that match the IGBP types (NB: mixed forest does not exist in ORCHIDEE as explicit vegetation type. Country abbreviations: E, Spain; P, Portugal; GB, Great Britain; I, Italy; B, Belgium; NL, Netherlands; D, Germany; F, France.

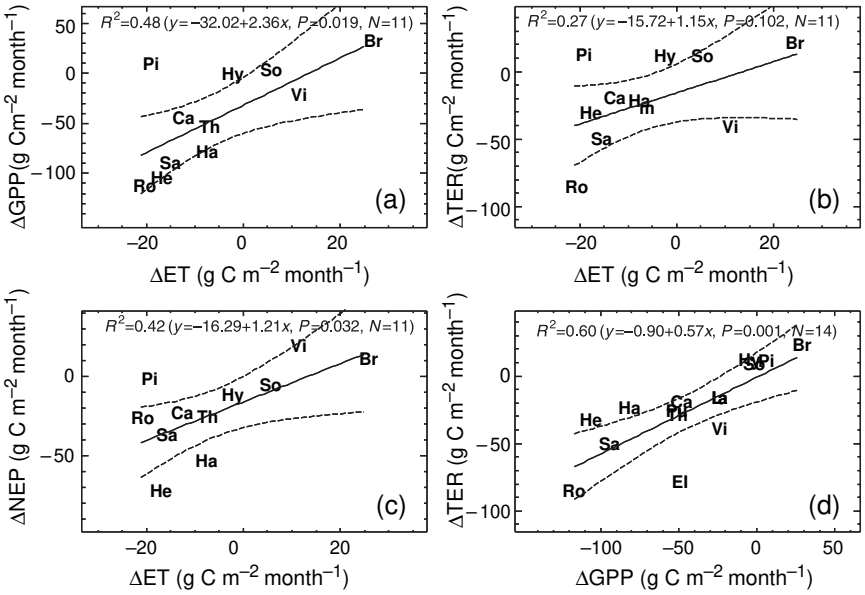

Fig. 6 Three correlation plots of year 2003 minus year 2002 differences of gross primary productivity (ΔGPP), ecosystem respiration (ΔTER) and net ecosystem productivity (ΔNEP) with respective evapotranspiration differences (ΔET), and one plot with the correlation between ΔTER and (ΔGPP). Anomalies are calculated for months July–September. Linear regression lines, 95% confidence bands and regression characteristics are indicated.

ORCHIDEE model reflects well the differential effect on the different countries (Pearson correlation of 0.90; Spearman's rank correlation of 0.64), but not on the different vegetation classes (Fig. 5b).

In some studies it is assumed that fAPAR (or NDVI) can be taken as a direct measure of productivity particularly in response to drought (e.g. Wylie *et al*., 2003). This has some justification for plant species that show little stomatal control of gas exchange, and consequently dry out and 'yellow' during a drought as some grass species. However, this cannot be generalized, and often radiation is absorbed and not fully used for CO_2 assimilation, but just dissipated, for example because the mesophyll concentration of CO_2 is too low due to closed stomata (Schäfer, 1994). This is particularly true for most tree species that control their leaf water balance. Consequently, the small changes of forest fAPAR (<3%) alone do not reflect the decrease in productivity that has been observed at the eddy covariance tower sites, often exceeding 40%. These observed decreases of productivity are caused by physiological reactions of the vegetation (stomatal control, enzyme activity) that hardly affect the fAPAR, but that might be detected via other indices like PRI.

The physiological control of gas exchange generally leads to a strong coupling of carbon and water fluxes at leaf and ecosystem level (Ball *et al*., 1987; Valentini *et al*., 1991). This is also evident here at the three-monthly scale, even with between-year flux differences (Fig. 6a). A correlation of interannual flux *differences* cannot be expected as high as e.g. hourly, daily or monthly flux correlations, where part of the correlation can be attributed to background correlation merely with the seasonal and diurnal cycles. Thus, a significant correlation of nearly 0.7 ($r^2 = 0.48$) [without the Pianosa site 0.89 ($r^2 = 0.79$, $P < 0.01$)] between the GPP and ET differences should be considered as a strong indication of the linkage between the carbon and water cycles, in addition to what is known from the seasonal scale. The Pianosa site however teaches us that this correlation can breakdown in the case of unproductive sites, where a lot of water is lost via 'unproductive' soil evaporation. Clearly, the partitioning of the evapotranspiration into 'productive' transpiration and 'unproductive' evaporation also depends on the distribution and timing of the rain events: if rainfall comes in many small events a larger fraction is intercepted or evaporated from the soil surface and a small fraction is penetrating into the soil and available for roots. Thus, a relation between GPP and ET being as strict as at the single-plant level cannot be expected at the ecosystem level.

A correlation of ecosystem respiration with evapotranspiration can be hypothesized from two different perspectives: First, as TER and GPP are linked (Fig. 6d) and GPP and ET, a correlation of TER with ET should be expected. Second, evapotranspiration is an indicator of the available energy and water availability that in turn relate to ecosystem respiration. The empirical correlation between the TER and ET differences is weaker than

with the productivity (Fig. 6b), and only significant again, if the Pianosa site is excluded ($r = 0.69$, $r^2 = 0.48$, $P < 0.05$). It is also worthwhile noting that for all regressions with ΔET the intercept is slightly negative (Fig. 6a–c), suggesting there might be another factor not related to the water cycle reducing the ecosystem productivity. For instance increased levels of ozone have been observed during summer 2003 (R. Vautard, personal communication) that can have impaired plant photosynthesis.

Another question is related to what factor drove the reaction of the biosphere to the climate anomaly. Certainly an empirical-statistical analysis cannot give a final answer, but Fig. 7, where all ecosystem fluxes were more closely related to water deficit than to temperature effects, strongly suggests that the biosphere has

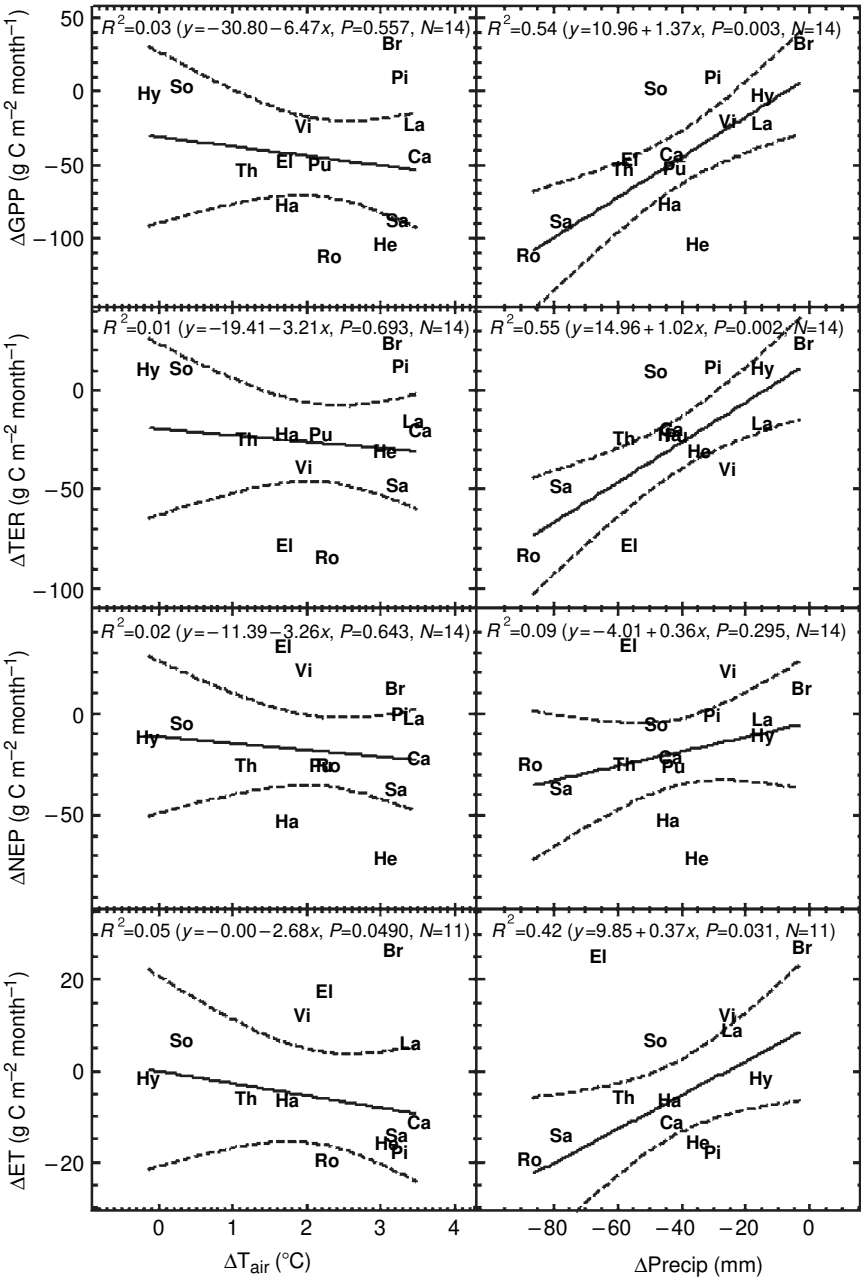

Fig. 7 Correlation plots of year 2003 minus year 2002 differences of gross primary productivity (ΔGPP), ecosystem respiration (ΔTER), net ecosystem productivity (ΔNEP) and evapotranspiration (ΔET) with respective temperature (ΔT_{air}) and precipitation (ΔPrecip) differences. Anomalies are calculated for months July–September, except for precipitation that are for June–August to better account for lag effects. Linear regression lines, 95% confidence bands and regression characteristics are indicated.

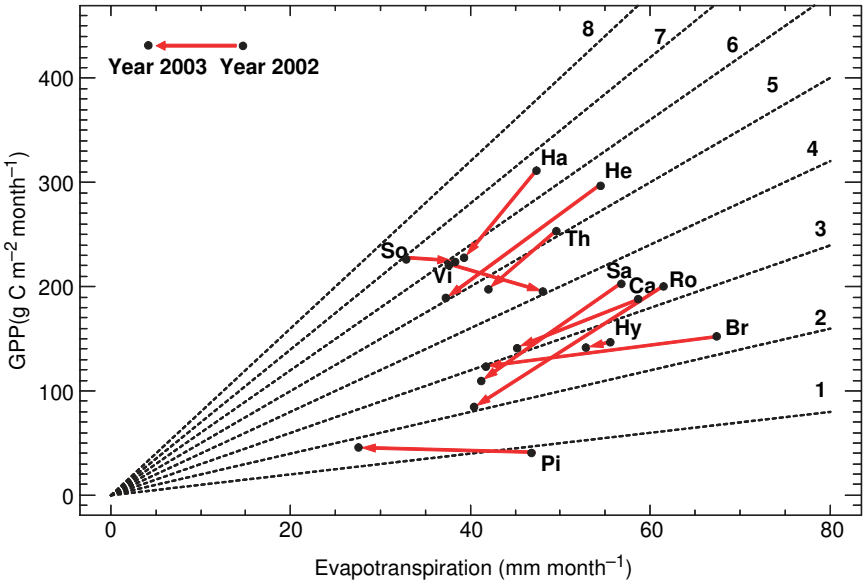

Fig. 8 Average gross primary productivity (GPP) vs. evapotranspiration (ET) for the different sites during July–September 2002 and 2003. Labels include the sites code and are located at year 2002, while the red arrow points to year 2003. Dashed lines represent GPP/ET ratios from 1 to 8 g C kg^{-1} H_2O.

'perceived' the summer 2003 rather as a drought than a heat wave. Related to this is the fact that obviously the theoretically expected positive direct effects of temperature on respiration and evapotranspiration cannot be found in the data (Fig. 7c, g) (i.e. is overridden by the drought effect). Also in multivariate regressions involving precipitation and air temperature differences, the latter do not add significant explanatory power in any case with respect to GPP, NEP, R_{eco} or ET, and increase the explained variance only by maximally 4% points (e.g. from 54% to 58% in the case of GPP).

The strong sensitivity of the carbon fluxes to water limitation imposes the question about how WUE has been affected in the summer of 2003 (Fig. 8). While there are obviously clear between-site differences in WUE, it is remarkable that (among the sites with lower fluxes in 2003) all sites but Pianosa and Vielsalm show an almost parallel trajectory in the GPP-ET space from 2002 to 2003 with a slight decrease in WUE. This feature nicely materializes when plotting WUE in 2002 against WUE in 2003 (Fig. 9), which almost fall on one line slightly above the $y = x$-line, emphasizing that WUE seems relatively conservative within one site and tends to decrease towards a drier year. As has been shown in Reichstein *et al.* (2002) this pattern challenges many current ecosystem model formulations, where pure stomatal control implies increasing WUE under soil drying conditions (Schulze *et al.*, 2005).

The preliminary model intercomparison of gross ecosystem production (GEP) explores the range of possible modelling results caused by a number of factors, with varying meteorological input, different temporal and spatial resolution and different model type (process- vs. data-oriented), although not systematically. Major patterns described by all modelling approaches are the circum-Alpine negative GPP anomaly with an emphasis in northern and westerly directions, the relatively unaffected Iberian Peninsula and a positive anomaly over western Scandinavia (Fig. 10a). Smaller scale pattern descriptions at some places slightly deviate between models (e.g. eastern Scandinavia, United Kingdom, Balkan, North-Western France) but also similar patterns like transitional patterns along Italy are remarkable. The differences between the model outputs are depicted in Fig. 10b, where pixel-by-pixel between-model standard deviations are shown highlighting large model differences in Eastern Europe, but otherwise moderate deviations between the models. It has to be noted that part of the variability is due to differences in the meteorological drivers, which has to be sorted out in a more formal subsequent model inter-comparison. At some instances large standard deviations are caused by a single model also (e.g. spot in Sweden caused by ORCHIDEE and there caused by the ECMWF data input). Although driven by (smoothed) coarse $1^\circ \times 1^\circ$ meteorological data, the diagnostic modelling approaches (MOD17, ANN) show a high-resolution arrangement of the GPP anomaly that is clearly an imprint of the observed fPAR pattern (cf. Fig. 2). For instance, the local effect of the Portuguese forest fires is seen in the remote sensing

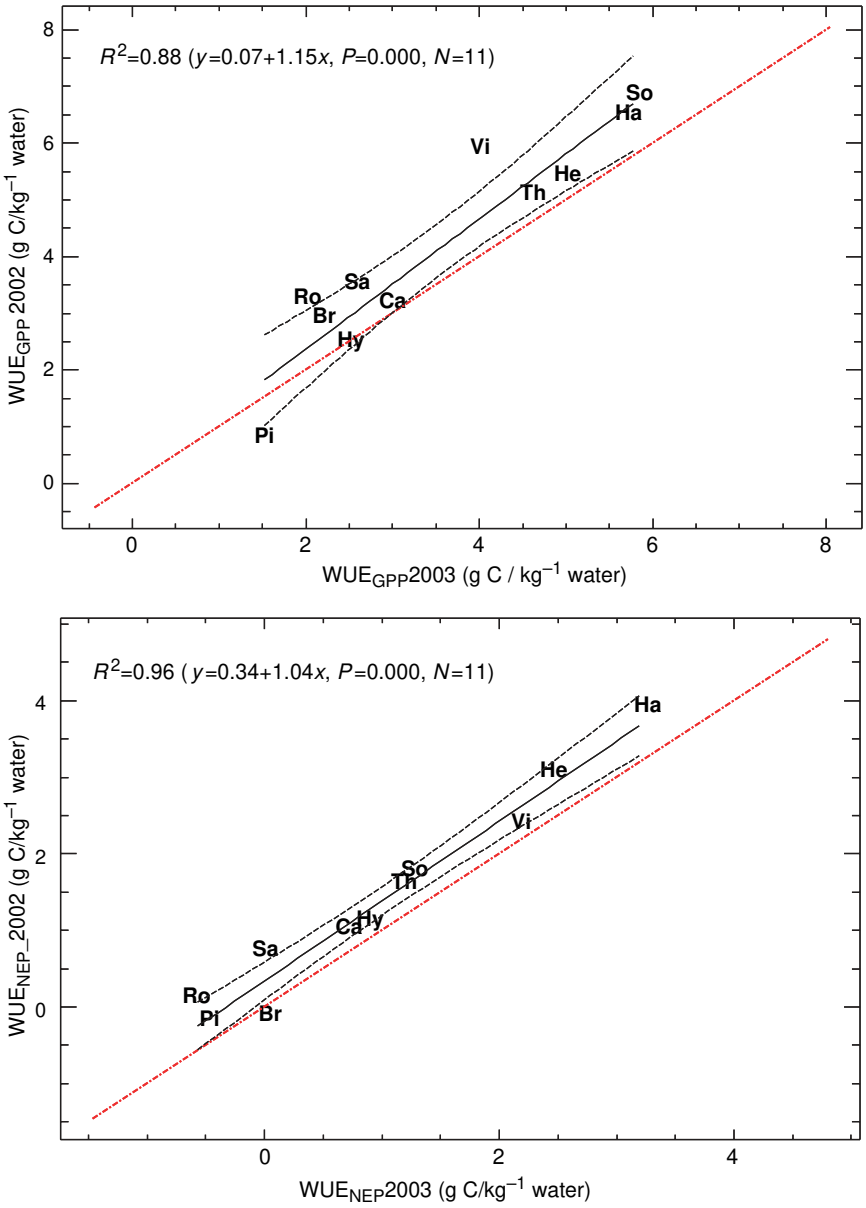

Fig. 9 Water-use efficiencies during July–September 2002 vs. 2003 for each site. Upper panel is the water-use efficiency of gross primary productivity, lower panel of net ecosystem productivity. Linear regression lines, 95% confidence bands, regression characteristics are indicated. Red line is the 1:1-line.

driven model while certainly the process-driven models cannot predict those stochastic events (and do not aim at this).

While we do not focus on a detailed process-based model evaluation at site level in this study, at least it is important to note that the models did differently response to the temperature and precipitation anomalies in 2003 (Fig. 11). In accordance with the observations, the process-based model GPP is more strongly related to precipitation than to the temperature differences between 2003 and 2002, while the MOD17 model seems to give similar weight to both temperature and precipitation anomalies affecting GPP. This is plausible since the standard MOD17 model does not use precipitation as a driving variable, but correlation between patterns of VPD (that is input to MOD17) and precipitation will have still caused a correlation between precipitation and MOD17-GPP.

Nevertheless, the overall model agreement (Fig. 10), where between model standard deviations are largely below 25 g C m^{-2}, is encouraging with respect to our ability to infer biospheric reactions to climate anoma-

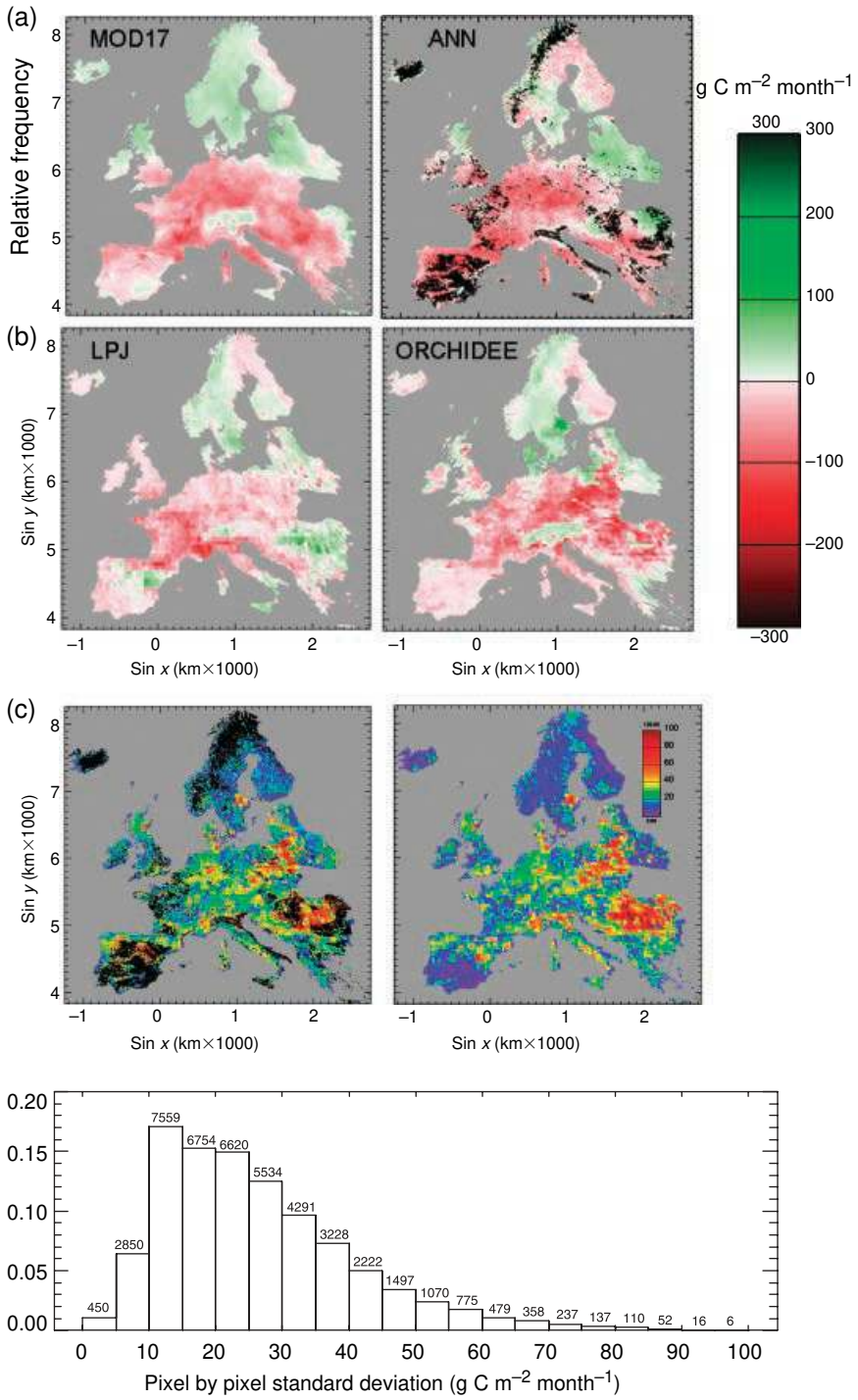

Fig. 10 (a) Spatially distributed modelled GPP anomalies in July–September 2003, with the Orchidee, MOD17, LPJ, and artifical neural network (ANN) models. Projection is sinusoidal centered at 0° longitude. (b) Between-model standard deviation of the predicted anomaly, left: including the ANN (black where no forest, and no ANN estimates available); right: excluding the ANN. (c) Histogram of pixel-by-pixel between-model standard deviation. 55% of the pixel exhibit standard deviations of less than 25 g C m^{-2} month^{-1}.

lies, having in mind the fact that between model variability is due to very different model structures, vegetation maps, meteorological drivers and resolution, thus, approximating the total uncertainty in modelling interannual variability. The general agreement of the very different model systems is also expressed in Fig. 12,

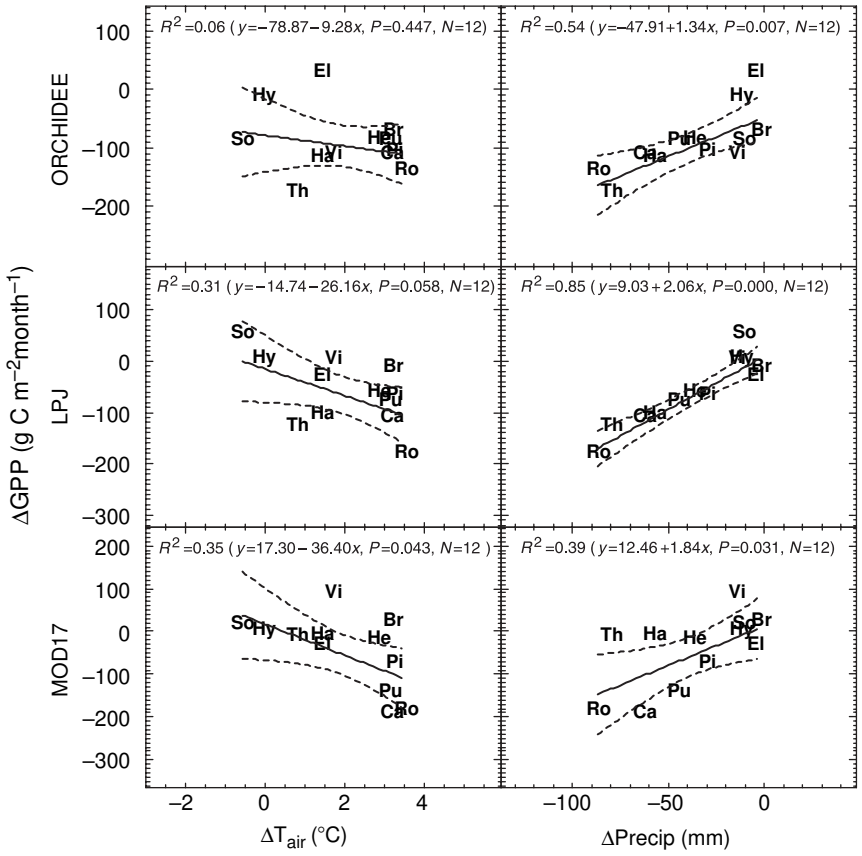

Fig. 11 Correlation plots of year 2003 minus year 2002 differences of gross primary productivity (ΔGPP), modelled at the eddy covariance sites by the ORCHIDEE, LPJ and MOD17 model with respective temperature (ΔT_{air}) and precipitation (ΔPrecip) differences (cf. Fig. 7). Anomalies are calculated for months July–September, except for precipitation that are for June–August to better account for lag effects. Linear regression lines, 95% confidence bands and regression characteristics are indicated.

where the spatially averaged summer anomaly of GPP and NEP over the central European domain is shown and all models associate the lowest productivity with the year 2003. The diagnostic models (particularly the ANN) exhibit a smaller variability in GPP than the process models, but with respect to NEP this is largely compensated by a lower ecosystem respiration variability yielding similar variability in NEP. It has to be sorted out how the differences between the models emerge; these could due to the models themselves or due to the different meteorological input. Hence, already at this stage the results are encouraging concerning our ability to model and detect climate impacts on the terrestrial biosphere.

Conclusions

From this study, we can draw conclusions from different perspectives. The remote sensing approach yields the only direct decadal view on the 2003 anomaly of the terrestrial biosphere via the observed reflectance expressed as fAPAR. Both the MODIS and the combined MODIS-AVHRR fAPAR time-series impressively proof the ability to detect the biosphere's response to extreme climate events and suggest that the summer 2003 was extremely abnormal not only in terms of meteorological conditions. However, only the dense network ecosystem observations within FLUXNET can provide a more precise picture on the functional response of ecosystems to extreme climate events. Most strikingly, we see a coordinated response of not only assimilatory (GEP) and dissimilatory (TER) processes but also of carbon and water fluxes, with very conservative WUE that are consistently lower during the summer 2003. Furthermore, we conclude from the statistical analysis of flux data that what has been perceived as a heatwave in the public was rather a drought spell for most of the biosphere.

From the modelling point of view the 2003 heatwave can be regarded as a proxy of future climate that will be warmer and with more extremes (Schär *et al.*, 2004). Hence, a successful modelling of the short-term effects

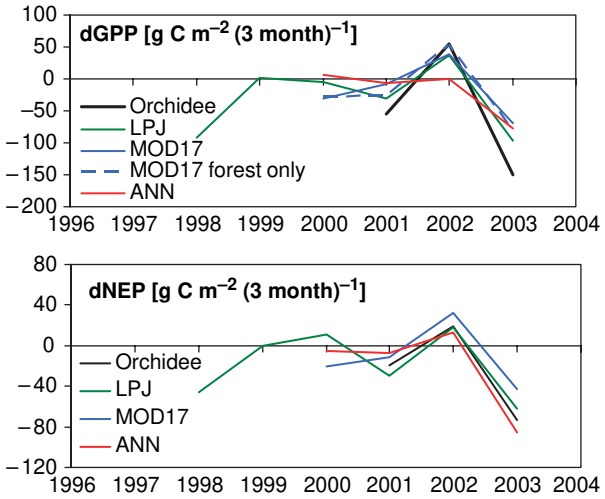

Fig. 12 Spatially integrated modelled summer gross primary productivity (GPP) (upper) and net ecosystem productivity (lower) anomalies with respect to the period 2000–2002. Spatial averaging was performed over the rectangular domain shown in Fig. 3. The dashed line for GPP shows the MOD17 anomaly averaging over forest pixels only, as such being directly comparable to the neural network result.

on the ecosystems carbon and water on the terrestrial ecosystem is a necessary (but not sufficient) condition for confidence of future model predictions. While the first model evaluation results are encouraging, this study however does not constitute a severe test of the different ecosystem models. Such a more severe test will be pursued by standardized model runs to understand if the climate sensitivity of ecosystem states and properties like WUE is well reproduced at site and continental level. An evaluation strategy that integrates process-level site network observations as in FLUXNET and spatial constraints as obtained via remote sensing merits sustained scientific attention in the future. A more severe test of the models including comparisons with the observed ecosystem fluxes and states at tower sites and with models driven by site meteorology needs to be pursued.

Acknowledgements

This study would have been impossible without the European Union funded projects CARBOEUROFLUX and CARBOEUROPE-IP. Flux tower measurements are part of the global FLUXNET network, which also has strongly stimulated integrated analysis of carbon and water flux data. During this study M.R. was supported by an Intraeuropean Marie Curie fellowship (MEIF-CT2003696) and a Independent Junior Research Grant from the German Max-Planck Society.

References

Aubinet M, Grelle A, Ibrom A *et al.* (2000) Estimates of the annual net carbon and water exchange of forests: the EUROFLUX methodology. *Advances in Ecological Research*, **30**, 113–175.

Baldocchi D, Falge E, Gu LH *et al.* (2001) FLUXNET: a new tool to study the temporal and spatial variability of ecosystem-scale carbon dioxide, water vapor, and energy flux densities. *Bulletin of the American Meteorological Society*, **82**, 2415–2434.

Ball JT, Woodrow IE, Berry JA (1987) A model predicting stomatal conductance and its contribution to the control of photosynthesis under different environmental conditions. In: *Progress in Photosynthesis Research. Proceedings of the VII International Photosynthesis Congress* (ed. Biggins I), p. 221–224.

Botta A, Viovy N, Ciais P *et al.* (2000) A global prognostic scheme of leaf onset using satellite data. *Global Change Biology*, **6**, 709–726.

Ciais P, Reichstein M, Viovy N *et al.* (2005) Europe-wide reduction in primary productivity caused by the heat and drought in 2003. *Nature*, **437**, 529–533.

Collatz CG, Ball JT, Grivet C *et al.* (1991) Physiological and environmental regulation of stomatal conductance, photosynthesis and transpiration: a model that includes a laminar boundary layer. *Agricultural and Forest Meteorology*, **54**, 107–136.

Demuth HB, Beale MH (2001) *Neural Network Toolbox User's Guide – For use with MATLAB v. 4*. The Mathworks Inc, Natick, USA.

Dijk A, Dolman AJ, Schulze E-D (2005) Radiation, temperature and leaf area explain ecosystem carbon fluxes in boreal and temperate European forests. *Global Biogeochemical Cycles*, **19**, GB2029, doi:2010.1029/2004GB002417.

Farquhar GD, Von Caemmerer S (1982) Modelling of photosynthetic response to environmental conditions. In: *Physiological Plant Ecology (Encyclopedia of Plant Physiology 12b)* (ed. Lange OL), p. 550–587. Springer, Berlin.

Foley JA, Prentice IC, Ramankutty N *et al.* (1996) An integrated biosphere model of land surface processes, terrestrial carbon balance, and vegetation dynamics. *Global Biogeochemical Cycles*, **10**, 603–628.

Friedl MA, McIver DK, Hodges JCF *et al.* (2002) Global land cover mapping from MODIS: algorithms and early results. *Remote Sensing of Environment*, **83**, 287–302.

Friedlingstein P, Joel G, Field CB *et al.* (1999) Towards an allocation scheme for global terrestrial carbon models. *Global Change Biology*, **5**, 755–770.

Goulden ML, Munger JW, Fan S-M *et al.* (1996) Measurements of carbon sequestration by long-term eddy covariance: methods and a critical evaluation of accuracy. *Global Change Biology*, **2**, 169–182.

Granier A, Reichstein M, Bréda N *et al.* (2005) The drought of 2003 in Western Europe: consequences on forest ecosystem functioning. *Agricultural and Forest Meteorology*, submitted.

Haxeltine A, Prentice IC (1996) A general model for the light-use efficiency of primary production. *Functional Ecology*, **10**, 551–561.

Haxeltine A, Prentice IC, Creswell DI (1996) A coupled carbon and water flux model to predict vegetation structure. *Journal of Vegetation Science*, **7**, 651–666.

Hunt ER, Piper SC, Nemani R *et al.* (1996) Global net carbon exchange and intra-annual atmospheric CO_2 concentrations

predicted by an ecosystem process model and three-dimensional atmospheric transport model. *Global Biogeochemical Cycles*, **10**, 431–456.

Joffre R, Rambal S, Ratte JP *et al*. (2005) Remote sensing of gypsy moth defoliation in evergreen Mediterranean oak forests. *Geophysical Research Abstracts*, **7**, 09035, SRef-ID: 01607-07962/gra/EGU09005-A-09035.

Jolly WM, Dobbertin M, Zimmermann NE *et al*. (2005) Divergent vegetation growth responses to the 2003 heat wave in the Swiss Alps. *Geophysical Research Letters*, **32**, doi:10.1029/2005GL023252.

Krinner G, Viovy N, de Noblet-Ducoudre N *et al*. (2005) A dynamic global vegetation model for studies of the coupled atmosphere-biosphere system. *Global Biogeochemical Cycles*, **19**, GB1015, doi: 1010.1029/2003GB002199.

Lloyd J, Taylor JA (1994) On the temperature dependence of soil respiration. *Functional Ecology*, **8**, 315–323.

Monteith JL (1995) Accomodation between transpiring vegetation and the convective boundary layer. *Journal of Hydrology*, **166**, 251–263.

Myneni RB, Hoffman S, Knyazikhin Y *et al*. (2002) Global products of vegetation leaf area and fraction absorbed PAR from year one of MODIS data. *Remote Sensing of Environment*, **83**, 214–231.

Nemani RR, Keeling CD, Hashimoto H *et al*. (2003) Climate-driven increases in global terrestrial net primary production from 1982 to 1999. *Science*, **300**, 1560–1563.

Papale D, Valentini R (2003) A new assessment of European forests carbon exhcanges by eddy fluxes and artificial neural network spatialization. *Global Change Biology*, **9**, 525–535.

Persson T, Oene Hv, Harrison T *et al*. (2000) Experimental sites in the NIPHYS/CANIF project. In: *Carbon and Nitrogen Cycling in European Forest Ecosystems. Ecological Studies 142* (ed. Schulze E-D), p. 20–35. Springer, New York.

Prentice IC, Cramer W, Harrison SP *et al*. (1992) A global biome model based on plant physiology and dominance, soil properties and climate. *Journal of Biogeography*, **19**, 117–134.

Reichstein M, Valentini R, Running S *et al*. (2004) Improving remote-sensing based GPP estimates (MODIS-MODI7) through inverse parameter estimation with CARBOEUROPE eddy covariance flux data. EGU meeting Nice 2004, Geophysical Research Abstracts 6:01388.

Reichstein M, Falge E, Baldocchi D *et al*. (2005) On the separation of net ecosystem exchange into assimilation and ecosystem respiration: review and improved algorithm. *Global Change Biology*, **11**, 1–16.

Reichstein M, Rey A, Freibauer A *et al*. (2003b) Modelling temporal and large-scale spatial variability of soil respiration from soil water availability, temperature and vegetation productivity indices. *Global Biogeochemical Cycles*, **17**, 15/11–15/15, doi: 10.1029/2003GB02035.

Reichstein M, Tenhunen J, Ourcival J-M *et al*. (2003c) Inverse modelling of seasonal drought effects on canopy CO_2/H_2O exchange in three Mediterranean Ecosystems. *Journal of Geophysical Research*, **108,** D23, 4726, 4716/4721–4716/4716, doi: 4710.1029/2003JD03430.

Reichstein M, Tenhunen JD, Ourcival J-M *et al*. (2002) Severe drought effects on ecosystem CO_2 and H_2O fluxes at three mediterranean sites: revision of current hypothesis? *Global Change Biology*, **8**, 999–1017.

Scardi M (2001) Advances in neural network modeling of phytoplankton primary production. Ecological Modelling. *Ecological Modelling*, **146**, 33–45.

Schäfer C (1994) Controlling the effects of excessive light energy fluxes: dissipative mechanisms, repair processes, and long-term acclimation. In: *Flux Control in Biological Systems* (ed. Schulze E-D), p. 37–56. Academic Press, San Diego.

Schär C, Vidale PL, Lüthi D *et al*. (2004) The role of increasing temperature variability in European summer heatwaves. *Nature*, **427**, 332–336, doi:310.1038/nature02300.

Schulze E-D, Beck E, Müller-Hohenstein K (2005) *Plant Ecology.* Springer Verlag, Heidleberg.

Sitch S, Smith B, Prentice IC *et al*. (2003) Evaluation of ecosystem dynamics, plant geography and terrestrial carbon cycling in the LPJ dynamic global vegetation model. *Global Change Biology*, **9**, 161–185.

Thornton PE, Law BE, Gholz HL *et al*. (2002) Modeling and measuring the effects of disturbance history and climate on carbon and water budgets in evergreen needleleaf forests. *Agricultural and Forest Meteorology*, **113**, 185–222.

Tucker CJ, Townsend JRG, Goff TE (1985) African landcover classification using satellite data. *Science*, **227**, 369–374.

Valentini R, Scarascia Mugnozza G, De Angelis P *et al*. (1991) An experimental test of the eddy correlation technique over a mediterranean macchia canopy. *Plant, Cell and Environment*, **14**, 987–994.

Viovy N, Arino O (1992) The best index slope extraction (BISE): a method for reducing noise in NDVI time-series. *International Journal of Remote Sensing*, **13**, 1585–1590.

Visual_Numerics_Inc. (2001) *PV-Wave Advantage Reference*. VNI Press, Houston.

Wang Q, Tenhunen J, Dinh NQ *et al*. (2004) Similarities in ground- and satellite-based NDVI time series and their relationship to physiological activity of a Scots pine forest in Finland. *Remote Sensing of Environment*, **93**, 225–237.

Wilson KB, Baldocchi DD, Aubinet M *et al*. (2002) Energy partitioning between latent and sensible heat flux during the warm season at FLUXNET sites. *Water Resources Research*, **38**, doi:10.1029/2001WR000989.

Wylie BK, Johnson DA, Laca E *et al*. (2003) Calibration of remotely sensed, coarse resolution NDVI to CO_2 fluxes in a sagebrush–steppe ecosystem. *Remote Sensing of Environment*, **85**, 243–255.

Zhou L, Kaufmann RK, Tian Y *et al*. (2003) Relation between interannual variations in satellite measures of northern forest greenness and climate between 1982 and 1999. *Journal of Geophysical Research-Atmospheres*, **108**, D1, 4004, doi: 4010.1029/2002JD02510.